SMA Technical Memo #163

Performance Assessment of a Beamformer for the Submillimeter Array

A. Young, R. Primiani, J. Weintroub, J. Moran, K. Young, L. Blackburn, M. Johnson, and R. Wilson

I. Introduction

Recently a new correlator was deployed at the Submillimeter Array (SMA) [1], called the SMA Wideband Astronomical ROACH2 Machine (SWARM) and developed on the Reconfigurable Open Architecture Hardware (ROACH2) architecture using the Collaboration for Astronomy Signal Processing and Electronics Research (CASPER) toolset [2]. In order to participate in Very Long Baseline Interferometry (VLBI) observations, this new digital backend is also equipped with a beamformer. This allows the connected element array to be phased up and join the wider VLBI array as a single station.

One challenge of phasing the array at submillimeter wavelengths is that the variability in the atmosphere, specifically in the distribution of water vapor, causes significant phase fluctuations in the signals output by each of the antennas. This variability, in both time and pointing direction, precludes the use of calibration methods that require steering the antennas off-source, and requires an in-situ calibration method where the beamformer weights are calculated while observing the source-of-interest. Such an algorithm, based on an analysis of the cross-correlation product output by the correlator was implemented and tested. Herein we describe the beamformer system, the algorithm used to calculate the weights, and present measured results to evaluate the overall performance.

II. Beamforming System

The digital backend samples a 1664 MHz wide IF signal at a rate of 3328 Msps[1] with 8-bit resolution. Processing includes doing coarse delay correction, calculating a 32768-point FFT, and applying the beamformer weights in the frequency-domain. From there the signal is fed to a correlator and a beamformer in parallel. The correlator output is sent to a computer which calculates updates for the beamformer weights vector that are fed back through a proportional-integral-differential (PID) loop, whereas the beamformed output is sent to a VLBI recorder. A functional description of the beamforming system is shown in Fig. 1.

[1]The system is currently running at 8/11 of the eventual rate of 4576 Msps.

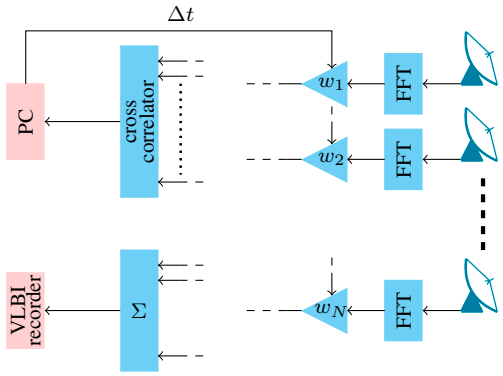

Fig. 1. Block diagram of the beamforming system. The SMA comprises of eight 6 m center-fed parabolic reflector antennas with a reconfigurable planar array layout. The array operates at 1.3 mm and shorter wavelengths.

III. Beamforming Algorithm

Let the frequency-domain voltage signal in antenna i be denoted as v_i,

$$v_i = s_i + n_i, \tag{1}$$

and be comprised of a signal-of-interest s_i and noise n_i component. The beamformer output b can then be expresed as

$$b = \mathbf{w}^H \mathbf{v} = \mathbf{w}^H \mathbf{s} + \mathbf{w}^H \mathbf{n} \tag{2}$$

where $\mathbf{w}$ is the weighting vector, and $\mathbf{v}$, $\mathbf{s}$ and $\mathbf{n}$ are the total, signal and noise array vectors, respectively. Steering the array towards the source-of-interest then requires $\mathbf{w} = \mathbf{s}$. Since the signal and noise components are independent the correlator output can be decomposed as

$$C = C_s + C_n, \tag{3}$$

where C_s and C_n are the signal and noise covariance matrices, respectively. For a point-like source the matrix C_s will be rank-1, with a single non-zero eigenvalue [3]. The associated eigenvector is equal to the array signal vector $\mathbf{s}$ within a scalar normalization factor. That is, if the signal covariance matrix can be determined from the total covariance matrix, the desired phasing vector $\mathbf{w} = \mathbf{s}$ can be recovered from the eigenvalue decomposition of C_s.

The noise component is uncorrelated among the antennas which means that the noise covariance matrix C_n is diagonal. Assuming that the gains of the antennas in the array are sufficiently matched, an approximation of C_s can then be determined by normalizing the elements in C to unit magnitude,

$$C_s' = \left\{ \frac{c_{ij}}{|c_{ij}|} \right\}. \tag{4}$$

The phasing vector is then calculated by solving

$$C_s' \mathbf{x} = \lambda \mathbf{x} \tag{5}$$

and selecting the vector $\mathbf{x}$ associated with the eigenvalue λ that has the largest real-valued component.

IV. Results

An on-sky test was performed in October 2015 to evaluate the performance of the beamforming system. During this test only seven of the eight antennas were used and the array was in the so-called extended configuration, with baseline lengths ranging between 44 m to 226 m. The sky frequency was tuned to 279.512 GHz. Two sources were observed during the test, 3C454.3 as a relatively strong source (spectral flux density of order 10 Jy), and 2155-152 which was somewhat weaker (spectral flux density of order 1 Jy). The sources were observed over a range of elevations between 25° and 70°, and the test was scheduled to run from shortly after sunset in order to test the system in relatively poor atmospheric conditions. The precipitable water vapor content of the atmosphere was in the range 1–1.5 mm (zenith opacity measured within the range 0.079–0.070), and weather reports showed clear skies with a wind speed of 2 m/s at the start of the test, and decreasing somewhat during the course of the night. The test was done in cycles of:

1) steering on-source with randomized constant phasing vector
2) turning on the phasing loop,
3) turning off the phasing loop, holding the last solution, and
4) steering off-source.

This procedure was executed two times on 3C454.3, then once on 2155-152, and then once more on 3C454.3. During the test the correlator accumulation period was set to 6.4 s.

The performance of the system was evaluated using phasing efficiency as the figure of merit,

$$\eta_\phi = \frac{\mathbf{w}^H \mathbf{s}}{\mathbf{s}^H \mathbf{s}}. \tag{6}$$

For an ideally phased array $\eta_\phi = 1$ and the effective area of the array will be equal to the sum of the effective areas of all the antennas. The measured phasing efficiency over the different portions of the October 2015 test are shown in Fig. 2. It is apparent in these tests that when the phasing loop is turned on after random phases have been applied there is a significant settling time (including some oscillations) before the phasing efficiency maximizes. This can be attributed to a well-known effect of the PID controller and can be minimized in the future through tuning of the PID weights. The tuning method might involve using historical data and a simulated beamformer for the sake of efficiency or may be done in real-time using a heuristic method. Except for the first cycle phasing efficiency is mostly above 0.9 once the phasing has settled, and the improvement over the course of the test is attributed to a stabilizing atmosphere. Once the feedback loop is switched off and the last computed phasing solution is held the efficiency deteriorates, more haphazardly for the earlier cycles than for the later cycles where the efficiency varies more smoothly and over a smaller range.

We have simulated the effects of a thin turbulent screen that moves across the array at the wind speed. The characteristics of the measured results can be reproduced with a Kolmogorov spectrum, characterized by a structure function that varies as the 5/3 power of the baseline length [4].

References

[1] P. T. Ho, J. M. Moran, and K. Y. Lo, "The submillimeter array," *The Astrophysical Journal Letters*, vol. 616, no. 1, p. L1, 2004.

[2] (2016) Collaboration for Astronomy Signal Processing and Electronics Research. [Online]. Available: https://casper.berkeley.edu/

[3] M. V. Ivashina, O. Iupikov, R. Maaskant, W. A. van Cappellen, and T. Oosterloo, "An optimal beamforming strategy for wide-field surveys with phased-array-fed reflector antennas," *Antennas and Propagation, IEEE Transactions on*, vol. 59, no. 6, pp. 1864–1875, 2011.

[4] C. Carilli and M. Holdaway, "Tropospheric phase calibration in millimeter interferometry," *Radio Science*, vol. 34, no. 4, pp. 817–840, 1999.

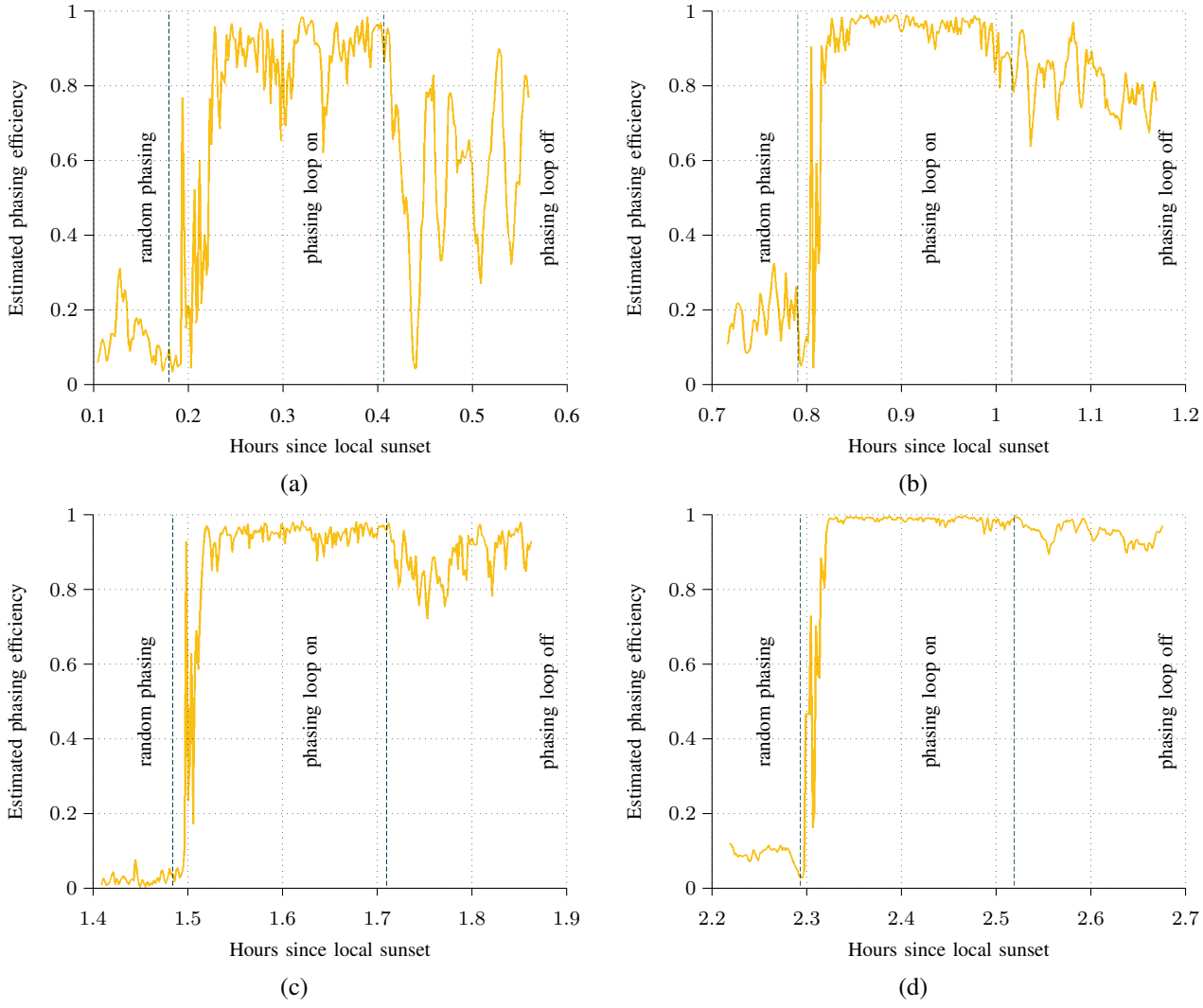

Fig. 2. Phasing efficiency versus time during (a) first cycle on 3C454.3, (b) second cycle on 3C454.3, (c) third cycle on 2155-152, and (d) fourth cycle on 3C454.3. The time is measured in hours since sunset in local time.